12th International Conference on Applications of Statistics and Probability in Civil Engineering, ICASP12
Vancouver, Canada, July 12-15, 2015

Compressive Polynomial Chaos Expansion for Multi Dimensional Model Maps

Stefano Marelli
Senior Assistant, Chair of Risk, Safety and Uncertainty ETH Zürich, Switzerland

Bruno Sudret
Professor, Chair of Risk, Safety and Uncertainty Quantification, ETH Zürich, Switzerland

ABSTRACT: Modern high-resolution numerical models used in engineering often produce multi-dimensional maps of outputs (*e.g.* nodal displacements on a FEM mesh) that may result in more than 10^5 highly correlated outputs for each set of model parameters. Most available metamodelling techniques, however, are not yet suitable for handling such large maps, including Polynomial Chaos Expansions (PCE). Indeed, the PCE of a numerical model with many outputs is traditionally handled by independently metamodelling each one of them. We introduce a two-stage PCE approach that aims at solving this problem: in the first stage, PCE is used to compress the map of outputs on a much sparser basis in the map coordinates; in the second stage, standard PCE of the compressed map is carried out w.r.t. the underlying model parameters. Standard PCE post-processing techniques are then used to derive analytical expressions for several stochastic properties of the resulting compressive PCE.

1. INTRODUCTION

Polynomial Chaos Expansions (PCE) are a well established tool in Uncertainty Quantification (UQ), in both applied mathematics and engineering applications. Extensive literature is available on efficient non-intrusive techniques for calculating the y_j coefficients, such as spectral projection and least-square regression (see *e.g.*, Sudret (2007) and references therein). However, a field of research that remains relatively unexplored is that of non-intrusive metamodelling of multi-dimensional model maps. Examples of such maps include time-dependent solutions of partial differential equations (PDE) and force/displacement fields calculated by finite element modelling FEM on multi-dimensional meshes. In their seminal work in the field of metamodelling of vector-valued functions, Blatman and Sudret (2013) proposed compressing the model response map via principal component analysis (PCA) and metamodelling each significant principal component independently. We herein propose an extension of this approach that uses PCE as the compression tool to represent complex (but regular) high-dimensional model maps efficiently. Due to the linearity of PCE, point-by-point convergence in the full-model space ensures similar convergence in the compressed model response.

In Section 2, we give a brief introduction to PCE for scalar and vector-valued functions. In Section 3, we introduce the concept of model maps and the formalism of compressive polynomial chaos expansions (CPCE). We also provide an algorithm for the non-intrusive calculation of the CPCE coefficients. In Section 4, we discuss and derive analytical expressions for several stochastic properties of CPCE. We then apply the CPCE on a test 2D function in Section 5. Finally, we summarize and give concluding remarks in Section 6.

2. POLYNOMIAL CHAOS EXPANSIONS

2.1. *Basic definitions*

Polynomial Chaos Expansion (PCE) is a spectral decomposition technique that allows one to represent a finite-variance scalar-output function $Y = \mathscr{M}(\boldsymbol{\Xi})$ as:

$$Y = \mathscr{M}(\boldsymbol{\Xi}) = \sum_{j=0}^{\infty} a_j \Psi_j(\boldsymbol{\Xi}) \qquad (1)$$

where $\boldsymbol{\Xi} \in \mathbb{R}^M$ is a random vector of uncertain parameters, $a_j \in \mathbb{R}$ is a set of scalar coefficients (spectral coordinates) and the $\Psi_j(\boldsymbol{\Xi}) \in \mathbb{R}$ form a polynomial orthonormal basis w.r.t. the functional scalar product:

$$\langle g(\boldsymbol{\xi}), h(\boldsymbol{\xi}) \rangle = \int_{\mathscr{D}_{\boldsymbol{\Xi}}} g(\boldsymbol{\xi}) h(\boldsymbol{\xi}) f_{\boldsymbol{\Xi}}(\boldsymbol{\xi}) d\boldsymbol{\xi} \quad (2)$$

where $\mathscr{D}_{\boldsymbol{\Xi}}$ is the support of $\boldsymbol{\Xi}$ and $f_{\boldsymbol{\Xi}}(\boldsymbol{\xi})$ is a positive semi-definite weight function that satisfies:

$$\int_{\mathscr{D}_{\boldsymbol{\Xi}}} f_{\boldsymbol{\Xi}}(\boldsymbol{\xi}) d\boldsymbol{\xi} = 1. \quad (3)$$

Note that, due to its properties, it is customary to interpret $f_{\boldsymbol{\Xi}}(\boldsymbol{\xi})$ as the probability density function (PDF) of the random variable $\boldsymbol{\Xi}$ in stochastic PCE applications. Nevertheless, the spectral decomposition in Eq. (1) is, in a more general context, a functional approximation of the model function $\mathscr{M}(\boldsymbol{\Xi})$ as long as an appropriate weight function $f_{\boldsymbol{\Xi}}(\boldsymbol{\xi})$ is used in the definition of the scalar product in Eq (2).

The orthonormality condition on the basis elements Ψ_j reads:

$$\left\langle \Psi_i(\boldsymbol{\Xi}), \Psi_j(\boldsymbol{\Xi}) \right\rangle = \delta_{ij}. \quad (4)$$

where δ_{ij} is the Kronecker symbol.

2.2. Sparsity of PCE

Note that the sum in Eq. (1) has an infinite number of terms, hence requiring truncation strategies for computational purposes. In practice, however, smooth models tend to have quickly decaying PCE coefficients, hence allowing for accurate basis truncation strategies to be devised. The truncated form of Eq. (1) reads:

$$Y(\boldsymbol{\Xi}) \simeq \sum_{\boldsymbol{\alpha} \in \mathscr{A}^{M,p}} a_{\boldsymbol{\alpha}} \Psi_{\boldsymbol{\alpha}}(\boldsymbol{\Xi}) \quad (5)$$

where $\boldsymbol{\alpha} = \{\alpha_1, \alpha_2, ..., \alpha_M\}$ is a multi-index that identifies the polynomial degree of $\Psi_{\boldsymbol{\alpha}}$ in each of the M input variables, while $\mathscr{A}^{M,p}$ is a finite cardinality $P = \left|\mathscr{A}^{M,p}\right|$ set of multi-indices of dimension M and maximum degree p.

The cardinality P can be controlled in many ways, *e.g.* via maximum-polynomial degree truncation strategies (*e.g.* hyperbolic truncation, see Blatman and Sudret, 2010) or via sparsity-favouring coefficient calculation strategies (*e.g.* through Least Angle Regression, Blatman and Sudret, 2011).

2.3. PCE of vector-valued models

A trivial extension of Eq. (1) to the case of models with vector-valued outputs $\boldsymbol{Y} = \left\{Y^1, Y^2, ..., Y^n\right\}$ consists in separately expanding each of the outputs independently on the same truncated basis:

$$Y^i(\boldsymbol{\Xi}) \simeq \sum_{\boldsymbol{\alpha} \in \mathscr{A}^{M,p}} a^i_{\boldsymbol{\alpha}} \Psi_{\boldsymbol{\alpha}}(\boldsymbol{\Xi}), \;\; i = 1, ..., n \quad (6)$$

Due to the orthonormality of the $\Psi(\boldsymbol{\xi})$ in Eq. (1) given in Eq. (4), it is trivial to demonstrate that the mean value of each of the components of $\boldsymbol{Y}$ is given by:

$$\mu^i_{\boldsymbol{Y}} = a^i_{\boldsymbol{0}} \quad (7)$$

where $a_{\boldsymbol{0}}$ represents the coefficient of the constant basis term. Correspondingly, the shared polynomial basis ensures that the covariance information between the elements of $\boldsymbol{Y}$ is also encoded in the coefficients $a^i_{\boldsymbol{\alpha}}$, even though they are calculated independently for each outputs. In fact, the covariance matrix of the elements of $\boldsymbol{Y}$ can be written as:

$$C^{ij}_{\boldsymbol{Y}} \overset{\text{def}}{=} \mathbb{E}\left[(Y^i - \mu^i_{\boldsymbol{Y}})(Y^j - \mu^j_{\boldsymbol{Y}})\right] \quad (8)$$

By substituting Eq. (6) and Eq. (7) into Eq. (8), one obtains (the reference to the random variable $\boldsymbol{\Xi}$ is dropped for better readability):

$$C^{ij}_{\boldsymbol{Y}} = \mathbb{E}\left[\sum_{\boldsymbol{\alpha} \neq \boldsymbol{0}} a^i_{\boldsymbol{\alpha}} \Psi_{\boldsymbol{\alpha}} \sum_{\boldsymbol{\beta} \neq \boldsymbol{0}} a^j_{\boldsymbol{\beta}} \Psi_{\boldsymbol{\beta}}\right] \quad (9)$$

where the notation $\boldsymbol{\alpha} \neq \boldsymbol{0}$ stands for $\boldsymbol{\alpha} \in \mathscr{A}^{M,p}_{\setminus \boldsymbol{0}}$.

Due to the orthonormality of the basis w.r.t. to the expectation value in Eq (4), it immediately follows that:

$$C^{ij}_{\boldsymbol{Y}} = \sum_{\boldsymbol{\alpha} \neq \boldsymbol{0}} a^i_{\boldsymbol{\alpha}} a^j_{\boldsymbol{\alpha}} \quad (10)$$

3. COMPRESSIVE POLYNOMIAL CHAOS

3.1. Model maps

In many common modelling scenarios, the model response to a sample of uncertain model parameters $\boldsymbol{\xi}$ is not simply a scalar, but it is a $d-$dimensional map, *e.g.* the displacements at the nodes of a complex finite element model (FEM). Hence, we define a *model map* as:

$$\mathscr{M}(\boldsymbol{\Xi}, \boldsymbol{X}) \in \mathbb{R} \quad (11)$$

where $\boldsymbol{\Xi} \in \mathbb{R}^M$ is a random vector with probability density function $f_{\boldsymbol{\Xi}}(\boldsymbol{\xi})$ that describes the uncertainty in the model parameters, while $\boldsymbol{X} \in \mathbb{R}^d$ is a set of coordinates in the appropriate model space (e.g., Cartesian coordinates, or time). An example of model map with $d = 1$ could be the vertical displacement along the length of a simply supported beam with uncertain Young's modulus. In this case, $\boldsymbol{X} \in \mathbb{R}$ would represent the coordinate along the beam length, while $\boldsymbol{\Xi}$ the uncertain Young's modulus.

Albeit strictly speaking not a random variable, a deterministic coordinate $\boldsymbol{X}$ on a bounded domain can be seen as a random variable suitably distributed on the entire map. In the case of a FEM model with a regular mesh, the node locations are uniformly distributed throughout the domain. Similarly, a finite-difference solution of a time-dependent PDE is typically calculated with regular time sampling.

In this contribution, we consider each calculation of a model map for a given realization $\boldsymbol{\xi}^{(i)}$ of the input random vector $\boldsymbol{\Xi}$ as a sample from a scalar model $\mathscr{M}(\boldsymbol{\xi}^{(i)}, \boldsymbol{X})$ with a d-dimensional random input vector $\boldsymbol{X}$. A $d = 2$ example of two realizations of such a map is shown for reference in Figure 1.

In typical applications, such sample can include several tens up to hundreds thousands of values, as is often the case with high fidelity FEM models. Very high resolutions, however, are often used due to numerical stability requirements, even in cases when the actual model response is very smooth. With no loss of generality, in this paper we will only consider applications where the sampling in the coordinate space is uniform. Note that there are no constraints in the regularity of the sampling, nor in the number of samples, which may even vary between different realizations of the random parameters $\boldsymbol{\xi}^{(i)}$, as long as their distribution is uniform.

3.2. Polynomial map compression

When metamodelling a function with a large number of outputs, the classical approach of performing full polynomial chaos expansion for each one of the outputs can quickly become impractical. Due to the independence of $\boldsymbol{\Xi}$ and $\boldsymbol{X}$, for any given realization $\boldsymbol{\xi}$ of the input random vector $\boldsymbol{\Xi}$, the truncated PCE in Eq. (5) of a model map realization on its coordinates can be written as follows:

$$\mathscr{M}(\boldsymbol{\xi}, \boldsymbol{X}) \simeq \sum_{\boldsymbol{\gamma} \in \mathscr{A}^{d,p_C}} c_{\boldsymbol{\gamma}}(\boldsymbol{\xi}) \boldsymbol{\Phi}_{\boldsymbol{\gamma}}(\boldsymbol{X}) \tag{12}$$

with orthonormal polynomial basis

$$\boldsymbol{\Phi}_{\boldsymbol{\gamma}}(\boldsymbol{X}) = \prod_{i=1}^{d} \phi_{\gamma_i}(X_i). \tag{13}$$

Please note that, due to the independence between $\boldsymbol{\Xi}$ and $\boldsymbol{X}$, the coefficients $c_{\boldsymbol{\gamma}}(\boldsymbol{\xi})$ are just scalars in the context of Eq. (12).

If the model map $\mathscr{M}(\boldsymbol{\Xi}, \boldsymbol{X})$ is smooth in the $\boldsymbol{X}$ coordinates, the number of coefficients $c_{\boldsymbol{\gamma}}(\boldsymbol{\xi})$ is typically limited to a few tens to several hundreds elements. Specifically, the number of coefficients equals the cardinality of the truncation set $P_C = |\mathscr{A}^{d,p_C}|$.

Considering each of the $c_{\boldsymbol{\gamma}}(\boldsymbol{\xi})$ as a function on the random input vector $\boldsymbol{\Xi}$, we can further expand each coefficient as:

$$c_{\boldsymbol{\gamma}}(\boldsymbol{\xi}) \simeq \sum_{\boldsymbol{\alpha} \in \mathscr{A}^{M,p}} a_{\boldsymbol{\gamma}\boldsymbol{\alpha}} \boldsymbol{\Psi}_{\boldsymbol{\alpha}}(\boldsymbol{\xi}) \tag{14}$$

which, when plugged back into Eq. (12) reads:

$$\mathscr{M}(\boldsymbol{\xi}, \boldsymbol{X}) \simeq \sum_{\boldsymbol{\gamma}} \sum_{\boldsymbol{\alpha}} a_{\boldsymbol{\gamma}\boldsymbol{\alpha}} \boldsymbol{\Psi}_{\boldsymbol{\alpha}}(\boldsymbol{\xi}) \boldsymbol{\Phi}_{\boldsymbol{\gamma}}(\boldsymbol{X}). \tag{15}$$

Equation (15) is the *compressive PCE equation* (CPCE). In case of a numerical smooth model map with a very large number of outputs for each realization of the random parameters $\boldsymbol{\xi}$, the outputs are first compressed to their sparse PCE coefficients, which in turn are surrogated via PCE on the original input random variables.

3.3. Non-intrusive calculation of the CPCE coefficients

Practically, the non-intrusive calculation of the coefficients $a_{\boldsymbol{\gamma}\boldsymbol{\alpha}}$ in Eq. (14) and Eq. (15) requires a two-step least-squares algorithm. For details about least-squares-based calculation of PCE coefficients, with emphasis on sparsity, please refer to Blatman and Sudret (2011).

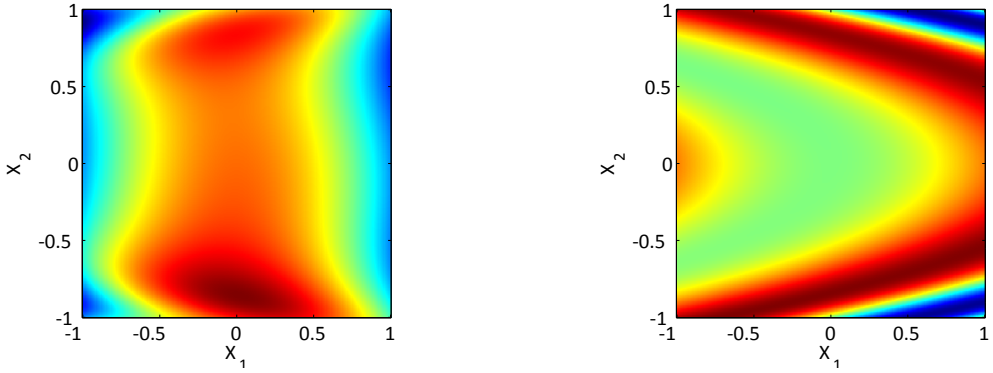

Figure 1: Two realizations of the model map in Eq. (23) *calculated on a regular grid with* $n = 10^5$ *nodes. Each map corresponds to one realization* $\boldsymbol{\xi}^{(i)}$ *of the input random vector* $\boldsymbol{\Xi}$.

In the first stage, an experimental design $\mathscr{E} = \left\{\boldsymbol{\xi}^{(1)}, \boldsymbol{\xi}^{(2)}, ..., \boldsymbol{\xi}^{(N)}\right\}$ is created as a suitably sized sample of the input random vector $\boldsymbol{\Xi}$, and the corresponding model maps are calculated $\mathscr{Y} = \left\{\boldsymbol{y}^{(1)}, \boldsymbol{y}^{(2)}, ..., \boldsymbol{y}^{(N)}\right\}$. Each $\boldsymbol{y}^{(i)}$ is a vector of scalar model responses at the corresponding set of coordinates $\mathscr{X}^{(i)} = \left\{\boldsymbol{x}^{(i)}_{(1)}, \boldsymbol{x}^{(i)}_{(2)}, ..., \boldsymbol{x}^{(i)}_{(n^{(i)})}\right\}$. Please note that there is no restriction on the size $n^{(i)}$ of each model map realization, as long as all map realizations are defined on the same domain and drawn from the same distribution. This property is important in practice, because many model maps have responses defined on coordinate sets that depend on the corresponding realization $\boldsymbol{\xi}^{(i)}$ of the random parameters $\boldsymbol{\Xi}$. A typical example would be the finite difference solution of a PDE in time, whose time-step (that defines the coordinates $\mathscr{X}^{(i)}$) depends on the model parameters to ensure numerical stability.

When the experimental design $\mathscr{Y}$ is available, a set of compressive PCE coefficients $\boldsymbol{c}^{(i)} = \{c_{\boldsymbol{\gamma}_1}(\boldsymbol{\xi}^{(i)}), c_{\boldsymbol{\gamma}_2}(\boldsymbol{\xi}^{(i)}), ..., c_{\boldsymbol{\gamma}_{P_C}}(\boldsymbol{\xi}^{(i)})\}$ is calculated according to Eq. (14) for each one of the experimental design samples $\boldsymbol{y}^{(i)}$. The coefficients are then grouped as $\mathscr{C} = \left\{\boldsymbol{c}^{(1)}, \boldsymbol{c}^{(2)}, ..., \boldsymbol{c}^{(N)}\right\}$. In a typical engineering scenario, $M \gg d$ and $n^{(i)} \gg N$, hence allowing the compression to achieve high accuracy in the coordinates $\boldsymbol{X}$ at a relatively low computational cost.

In the second stage, the compressed experimental design $\mathscr{C}$ is used to calculate the CPCE coefficients $a_{\boldsymbol{\gamma}\boldsymbol{\alpha}}$ in Eq. (14).

3.4. Considerations on convergence

Due to the linear nature of PCE, the compression coefficients $a_{\boldsymbol{\gamma}}(\boldsymbol{\xi})$ share similar properties of smoothness and finite variance as the original model map in equation Eq. (6). Hence, if the pointwise PCE on $\boldsymbol{\xi}$ of a model map is sparse and convergent for any $\boldsymbol{x}$, so will be its compressive counterpart in Eq. (15).

4. POST-PROCESSING OF CPCE

4.1. Moments of a CPCE

An important property of PCE is that its coefficients encode substantial information about the stochastic properties (*e.g.* moments) of the model response, as shown in Section 2.3. Due to the separation between physical coordinates and random input parameters in Eq. (12), the model map at each coordinate point $\boldsymbol{x}$ can be considered as a linear superimposition of the random variables $c_{\boldsymbol{\gamma}}(\boldsymbol{\xi})$ with coefficients $\boldsymbol{\Phi}(\boldsymbol{x})$. It is therefore easy to extend Eqs. (7) and (10) through Eq. (14):

$$\mu_{\boldsymbol{Y}}(\boldsymbol{x}) = \sum_{\boldsymbol{\gamma}} a_{\boldsymbol{\gamma}\boldsymbol{0}} \boldsymbol{\Phi}_{\boldsymbol{\gamma}}(\boldsymbol{x}) \tag{16}$$

for the mean value at a point $\boldsymbol{x}$. Correspondingly, the covariance between any two coordinate points $(\boldsymbol{x}, \boldsymbol{x}')$ reads:

$$C_{\boldsymbol{Y}}(\boldsymbol{x}, \boldsymbol{x}') = \sum_{\boldsymbol{\gamma}} \sum_{\boldsymbol{\gamma}'} C_{\boldsymbol{c}}^{\boldsymbol{\gamma}\boldsymbol{\gamma}'} \boldsymbol{\Phi}_{\boldsymbol{\gamma}}(\boldsymbol{x}) \boldsymbol{\Phi}_{\boldsymbol{\gamma}'}(\boldsymbol{x}') \tag{17}$$

where $C_{\boldsymbol{c}}^{\boldsymbol{\gamma}\boldsymbol{\gamma}'}$ is the covariance matrix of the random coefficients $\boldsymbol{c}_{\boldsymbol{\gamma}}(\boldsymbol{\xi})$ calculated according to

Eq. (10). Note that this result is equivalent to building a classical PCE in an augmented input space $\boldsymbol{\Xi}^{(\mathrm{aug})} = \{\boldsymbol{\Xi}, \boldsymbol{X}\}$. Such an approach, however, would be computationally more challenging, as it would require building a suitable PCE basis to account for the separability of the model map w.r.t. $\boldsymbol{\Xi}$ and $\boldsymbol{X}$, as well as solving a higher dimensional least squares minimization with a very large experimental design, instead of solving N independent, d-dimensional ones.

4.2. Variance decomposition and Sobol' indices

As demonstrated in Sudret (2008), a close relation exists between variance decomposition, and PCE coefficients. Such relation is particularly useful for the calculation of the so-called Sobol' global sensitivity indices, a well established tool in sensitivity analysis.

The basic form of variance decomposition can be written as follows (Sobol' (2001)):

$$\begin{aligned} f(\boldsymbol{\xi}) = &\sum_{i=1}^{M} f_i(\xi_i) + \sum_{i \neq j} f_{ij}(\xi_i, \xi_j) \\ &+ \ldots + f_{12\ldots M}(\xi_1, \xi_2, \ldots, \xi_M) + f_0 \end{aligned} \tag{18}$$

where the $f_{ij\ldots s}$ are scalar functions depending on the subset of input variables $\{\xi_i, \xi_j, \ldots, \xi_s\}$.

The coefficients in Eq. (14) can be grouped according to the functional dependence of the corresponding $\Psi_{\boldsymbol{\alpha}}$ (Sudret, 2008):

$$\begin{aligned} c_\gamma(\boldsymbol{\xi}) = &\sum_{\boldsymbol{\alpha} \in \mathscr{A}_i^{M,p}} a_{\boldsymbol{\gamma}\boldsymbol{\alpha}} \boldsymbol{\Psi}_{\boldsymbol{\alpha}}(\xi_i) + \sum_{\boldsymbol{\alpha} \in \mathscr{A}_{ij}^{M,p}} a_{\boldsymbol{\gamma}\boldsymbol{\alpha}} \boldsymbol{\Psi}_{\boldsymbol{\alpha}}(\xi_i, \xi_j) \\ &+ \ldots + a_{\boldsymbol{\gamma}\boldsymbol{\alpha}} \boldsymbol{\Psi}_{\boldsymbol{\alpha}}(\xi_i, \xi_j, \ldots, \xi_M) + \alpha_{\boldsymbol{\gamma}\mathbf{0}} \\ &\stackrel{\mathrm{def}}{=} c_{\boldsymbol{\gamma}}^{\{i\}} + c_{\boldsymbol{\gamma}}^{\{ij\}} + \ldots + c_{\boldsymbol{\gamma}}^{\{12\ldots M\}} + c_{\boldsymbol{\gamma}\mathbf{0}} \end{aligned} \tag{19}$$

where the set of multi-indices:

$$\begin{aligned} \mathscr{A}_{ij\ldots s}^{M,p} = \{ &\boldsymbol{\alpha} \in \mathscr{A}^{M,p} : \alpha_k > 0 \ \ \forall k \in \{i, j, \ldots s\}, \\ &\alpha_l = 0 \ \ \forall l \notin \{i, j, \ldots s\} \} \end{aligned} \tag{20}$$

identifies the basis elements that depend on the subset of the input variables $\{i, j, \ldots s\}$. Because of the uniqueness of the two representations in Eqs. (14) and (18), each sum in Eq. (18) can be identified with the corresponding sum in Eq. (19).

The Sobol' indices can be defined as the ratio of the variance of each term in Eq. (18) $D_{ij\ldots s}$ to the total variance D:

$$S_{ij\ldots s} = D_{ij\ldots s} / D. \tag{21}$$

By calculating the covariance matrices $C_{\boldsymbol{c}^{\{ij\ldots s\}}}^{\boldsymbol{\gamma}\boldsymbol{\gamma}'}$ of the sub-PCE compression coefficients $c_{\boldsymbol{\gamma}}^{\{ij\ldots s\}}$ in Eq. (19) with Eq. (10), it is trivial to derive the map-equivalent of the Sobol' indices in Eq. (21) starting from the map-covariance in Eq. (17):

$$S_{ij\ldots s}(\boldsymbol{x}) = \frac{1}{C_{\boldsymbol{Y}}(\boldsymbol{x}, \boldsymbol{x})} \sum_{\boldsymbol{\gamma}} \sum_{\boldsymbol{\gamma}'} C_{\boldsymbol{c}^{\{ij\ldots s\}}}^{\boldsymbol{\gamma}\boldsymbol{\gamma}'} \boldsymbol{\Phi}_{\boldsymbol{\gamma}}(\boldsymbol{x})^2. \tag{22}$$

5. EXAMPLE APPLICATION: 2D MAP

5.1. A 2D analytical map

To validate the method proposed and the corresponding post-processing properties, an ad-hoc complex 2D analytical map is created according to:

$$\begin{aligned} Y(\boldsymbol{\xi}, \boldsymbol{x}) = &e^{-\frac{1}{2}(x_1 \xi_1)} + 10 \xi_1^2 \xi_2 x_2^2 + \\ &\sin(-\pi(x_1^2 + \xi_2 x_2)^2) \end{aligned} \tag{23}$$

The map coordinates span a rectangular region $x_{1,2} \in [-1, 1]$. Each model evaluation returns the map value on a regular grid of 400×250 ($n = 10^5$) points in the coordinate space. Some example model maps for different realizations of $\boldsymbol{\Xi}$ are shown for reference in Figure 1.

The input random vector is chosen as $\boldsymbol{\Xi} \sim \mathscr{U}(-1, 1)^2$. Albeit in this particular case both the bounds and the dimensionality on $\boldsymbol{\Xi}$ and $\boldsymbol{X}$ coincide, this condition is neither required nor recommended. Indeed, in many typical engineering scenarios, $M \gg d$.

The choice of such a seemingly complex model stems from the need to meet the following criteria for demonstration purposes:

- the dimensionalities M and d must be low enough to allow for effective visualization;
- the model must be sufficiently complex and not simply polynomial;

- the model must exhibit sufficient variance *w.r.t.* the random inputs $\boldsymbol{\Xi}$;

- the model must have predictable distributions for moments and sensitivity indices.

5.2. The experimental design

The experimental design used in this analysis consists of $N = 200$ realizations of the input random vector $\boldsymbol{\Xi}$, hence resulting in a corresponding number of model maps similar to those in Figure 1.

Following the approach outlined in Section 3.3, the set of model responses $\mathscr{Y}$ is calculated on the experimental design $\mathscr{E} = \left\{\boldsymbol{\xi}^{(1)}, \boldsymbol{\xi}^{(2)}, ..., \boldsymbol{\xi}^{(N)}\right\}$. The corresponding set of compressive- experimental designs in the map coordinates $\mathscr{X}^{(i)} \equiv \mathscr{X} = \left\{\boldsymbol{x}_{(1)}, \boldsymbol{x}_{(2)}, ..., \boldsymbol{x}_{(n)}\right\}$ is identical for each experimental design sample $\boldsymbol{\xi}^{(i)}$: the regular grid with $n = 10^5$ nodes described in Section 5.1.

5.3. Experimental design compression

For the calculation of the compressive coefficients $\boldsymbol{c_\gamma}$ in Eq. (14), the regular grid $\mathscr{X}$ is treated as a uniform sampling of a random vector $\boldsymbol{X} \sim \mathscr{U}(-1,1)^2$. Ordinary least squares regression with maximum polynomial degree $p_c = 25$ in $d = 2$ dimensions is then performed. A hyperbolic truncation scheme with $q = 0.7$ is chosen to define the PCE basis (Blatman and Sudret, 2011). The choice of p_c and q is based on a preliminary analysis of a random subset of the available experimental design. More generally, it is possible to apply any adaptive sparse PCE algorithms to determine the smallest set of basis elements suitable to accurately represent all the maps in the experimental design. The resulting estimated generalization error for each element of the experimental design was observed in the range $err_G \in [10^{-14},\ 10^{-6}]$, indicating excellent compression accuracy.

The coefficients of the N PCEs thus calculated are gathered in the compressed design $\mathscr{C} = \left\{\boldsymbol{c}^{(1)}, \boldsymbol{c}^{(2)}, ..., \boldsymbol{c}^{(N)}\right\}$. After compression, the original representation of each experimental design sample was reduced from $n = 10^5$ to a much more manageable $n_c = |\mathscr{A}^{d,p_c}| = 226$ scalars.

5.4. Compressive PCE

Classical PCE is now performed independently for each of the n_c dimensions of $\mathscr{C}$ to calculate the $a_{\boldsymbol{\gamma\alpha}}$ coefficients in Eq. (15). For this application, we performed sparse adaptive PCE using the Least Angle Regression algorithm (LARS) to enforce $L1$ sparsity on the set of coefficients. The polynomial degree was adaptively chosen for each of the output dimensions in the range $p \in [3,15]$ (for degree-adaptive LARS, see Blatman and Sudret, 2011). The final accuracy of this expansion varied from acceptable to good, with $err_{G\boldsymbol{\gamma}} \in [10^{-4},\ 10^{-3}]$.

5.5. CPCE results

Finally, a validation set of $N_{\text{val}} = 10^4$ samples obtained by crude Monte Carlo simulation is evaluated with the full model in Eq. (23) to compare the statistical properties of the model map with those extracted from the coefficients of the CPCE.

Expectation value: the reference expectation value of the map calculated from the validation set is shown in the left panel of Figure 2. The corresponding CPCE-based estimate calculated with Eq. (16) is shown in the right panel of the same figure. The match between the two is excellent in all the points in the map coordinates $\boldsymbol{X}$.

Variance: the variance of the map is shown on the left panel of Figure 3, while the corresponding PCE approximation (Eq. (17)) is shown in the right panel of the same Figure. The approximation is once again excellent throughout the domain.

Sobol' indices: the calculation of Sobol' indices for such a large map would be by far too expensive with classical methods. CPCE, however, provides a functional form of the Sobol' indices in Eq. (22), which can be used to inexpensively calculate them for the entire map, even in points that are not included in the outputs of the original model. Figure 4 shows the full maps of Sobol' indices on the domain of $\boldsymbol{X}$. For validation purposes, we show in Figure 5 the comparison between several point-wise PCEs and CPCE for a slice at $x_2 \simeq -0.25$. The Sobol' indices calculated from point-wise PCE are plotted as circles, while the corresponding estimates by CPCE by solid lines. The match is excellent.

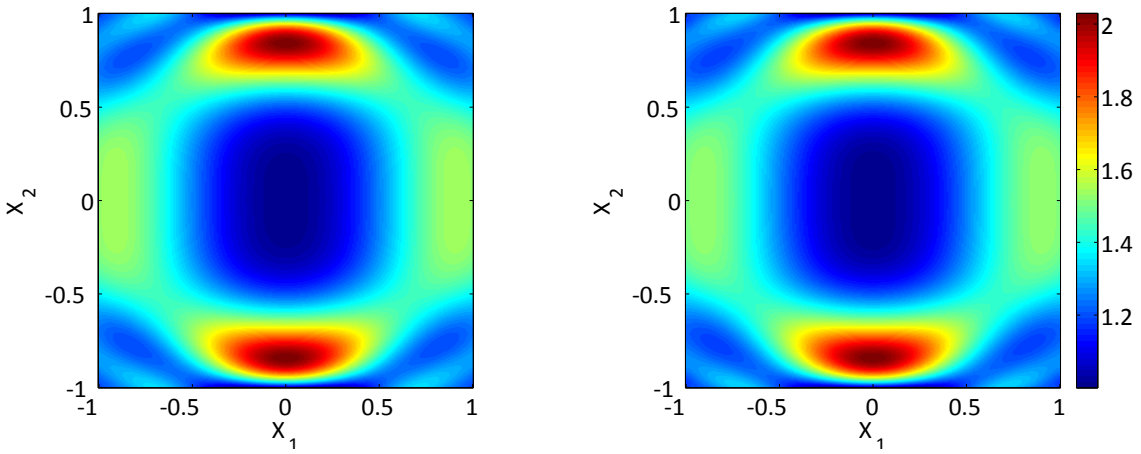

Figure 2: Mean map of the model in Eq. (23) *as calculated from a reference sampling (left) and its estimate from PCE coefficients based on Eq.* (16) *(right).*

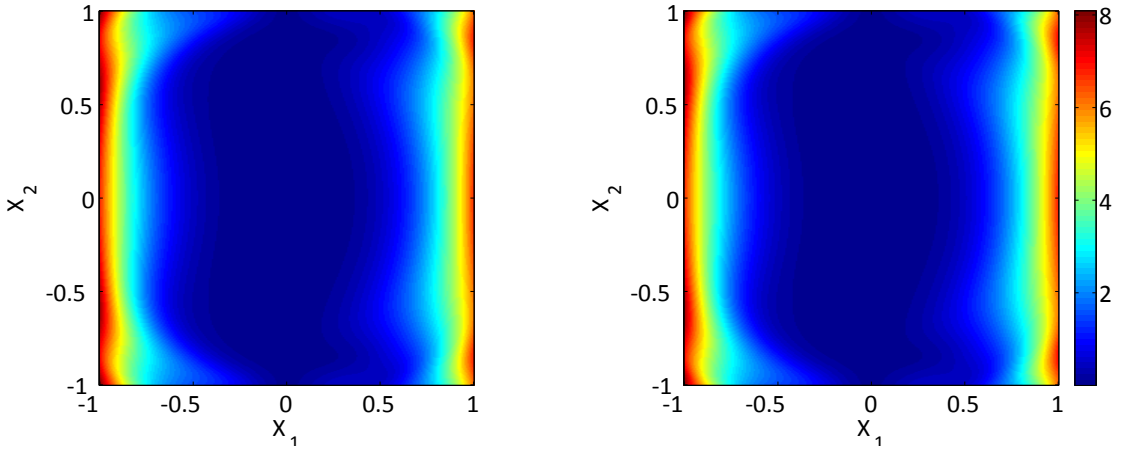

Figure 3: Variance map of the model in Eq. (23) *as calculated from a reference sampling (left) and its estimate from PCE coefficients based on Eq.* (17) *(right).*

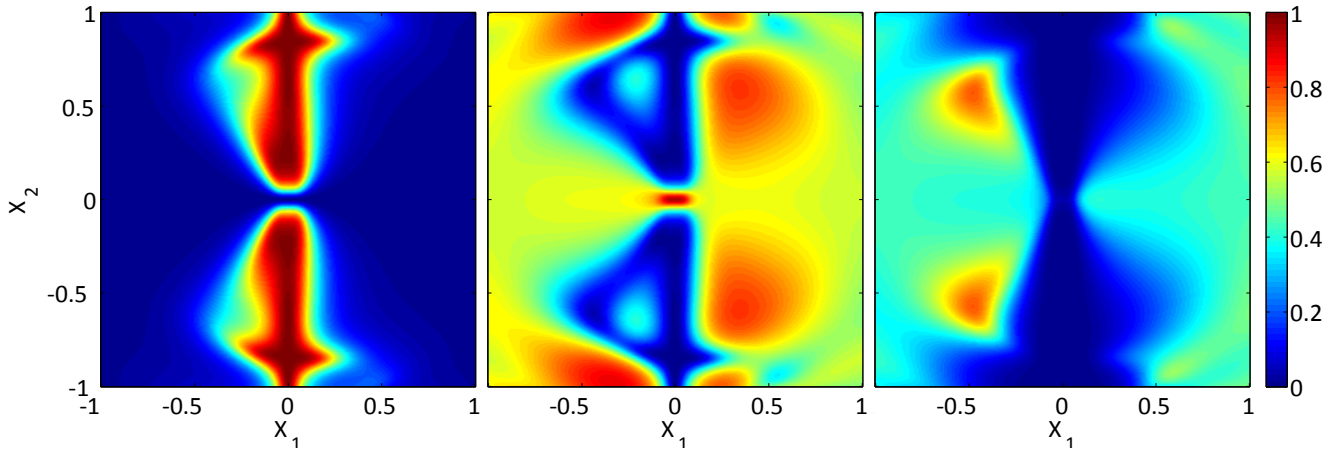

Figure 4: First order Sobol' index maps for ξ_1 (left) and ξ_2 (center) as estimated with Eq. (22) *and corresponding second order index map (right).*

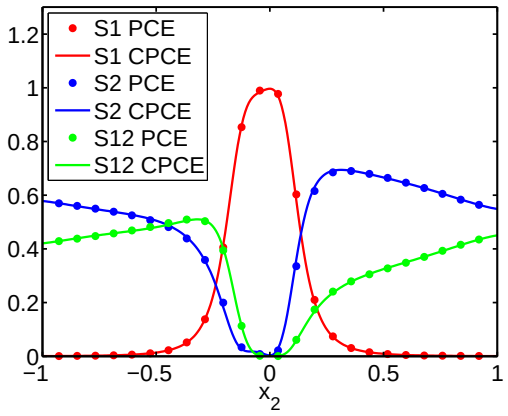

Figure 5: Comparison between Sobol' indices calculated with point-wise PCE and CPCE on a vertical slice at $x_2 = -0.25$.

6. SUMMARY AND CONCLUSIONS

In this paper we have introduced an algorithm that leverages on the regularity of numerical models with a large number of outputs by adopting a compression strategy. In particular, it is well known that PCE has very good sparsity properties for smooth functions on bounded domains. Therefore, we introduced a two-stage approach to first pre-process the experimental design of model maps, compressing it on a sparse PCE basis, followed by classical PCE on the compressed experimental design.

Due to the linearity of PCE, we could derive simple analytical expressions for the functional representation of the first moments of the model map in terms of its coordinates, as well as for more complex (and interesting) quantities that can be normally derived by post-processing PCE coefficients.

We want to stress on the fact that this approach does not degrade nor improve the convergence properties of classical point-wise PCE. This is important, as CPCE does not aim at extending the validity class of PCE methods, but rather at allowing the analyst to handle models with a large number of outputs. It is common engineering practice *e.g.* to calculate expensive FEM responses of complex structures, but then to only consider few selected quantities of interest for their actual analysis (*e.g.* selected inter-storey displacements, etc.). With CPCE, the entire set of displacements could be meta-modelled, hence taking advantage of the complexity of the full calculation.

Finally, it should be noted that the choice of PCE as the compression tool is just one of many: the only requirement for the entire formal setting of this paper is that the spectral representation in Eq. (12) holds. Polynomials are one of a number of orthonormal bases that can be built to represent a d-dimensional scalar function as a linear superimposition of terms. Other commonly employed spectral techniques include Fourier transforms, orthogonal wavelet decomposition, Karhunen-Loève expansions and many others. Note that standard finite element representation is also part of this framework. In other words, any spectral decomposition on an orthonormal basis onto which each realization of the model map is smooth can be used within this framework with the same equations.

Future extensions of this work include the combination of the prediction errors from the two stages of PCE to the final map, as well as a more efficient compression strategy that only considers significant terms in the truncated set $\mathscr{A}^{d,p_c}$.

REFERENCES

Blatman, G. and Sudret, B. (2010). "An adaptive algorithm to build up sparse polynomial chaos expansions for stochastic finite element analysis." *Prob. Eng. Mech.*, 25(2), 183–197.

Blatman, G. and Sudret, B. (2011). "Adaptive sparse polynomial chaos expansion based on Least Angle Regression." *J. Comput. Phys*, 230, 2345–2367.

Blatman, G. and Sudret, B. (2013). "Sparse polynomial chaos expansions of vector-valued response quantities." *Proc. 11th Int. Conf. Struct. Saf. Reliab. (ICOSSAR'2013), New York, USA*, G. Deodatis, ed.

Sobol', I. (2001). "Global sensitivity indices for nonlinear mathematical models and their Monte Carlo estimates." *Math. Comput. Simul.*, 55(1-3), 271–280.

Sudret, B. (2007). "Uncertainty propagation and sensitivity analysis in mechanical models - Contributions to structural reliability and stochastic spectral methods." *Habilitation thesis*, Université BLAISE PASCAL - Clermont II.

Sudret, B. (2008). "Global sensitivity analysis using polynomial chaos expansions." *Reliab. Eng. Sys. Saf.*, 93, 964–979.